

REPORT DOCUMENTATION PAGE			Form Approved OMB NO. 0704-0188		
<p>The public reporting burden for this collection of information is estimated to average 1 hour per response, including the time for reviewing instructions, searching existing data sources, gathering and maintaining the data needed, and completing and reviewing the collection of information. Send comments regarding this burden estimate or any other aspect of this collection of information, including suggestions for reducing this burden, to Washington Headquarters Services, Directorate for Information Operations and Reports, 1215 Jefferson Davis Highway, Suite 1204, Arlington VA, 22202-4302. Respondents should be aware that notwithstanding any other provision of law, no person shall be subject to any penalty for failing to comply with a collection of information if it does not display a currently valid OMB control number. PLEASE DO NOT RETURN YOUR FORM TO THE ABOVE ADDRESS.</p>					
1. REPORT DATE (DD-MM-YYYY) 10-03-2017		2. REPORT TYPE Final Report		3. DATES COVERED (From - To) 10-May-2016 - 9-Feb-2017	
4. TITLE AND SUBTITLE Final Report: Research Area 11.1: HCP Mg Alloys Formable at Room Temperature			5a. CONTRACT NUMBER W911NF-16-1-0294		
			5b. GRANT NUMBER		
			5c. PROGRAM ELEMENT NUMBER 611102		
6. AUTHORS Semyon Vaynman, Yip-Wah Chung, Dieter Isheim			5d. PROJECT NUMBER		
			5e. TASK NUMBER		
			5f. WORK UNIT NUMBER		
7. PERFORMING ORGANIZATION NAMES AND ADDRESSES Northwestern University Evanston Campus 1801 Maple Avenue Evanston, IL 60201 -3149			8. PERFORMING ORGANIZATION REPORT NUMBER		
9. SPONSORING/MONITORING AGENCY NAME(S) AND ADDRESS (ES) U.S. Army Research Office P.O. Box 12211 Research Triangle Park, NC 27709-2211			10. SPONSOR/MONITOR'S ACRONYM(S) ARO		
			11. SPONSOR/MONITOR'S REPORT NUMBER(S) 69187-MS-II.1		
12. DISTRIBUTION AVAILABILITY STATEMENT Approved for Public Release; Distribution Unlimited					
13. SUPPLEMENTARY NOTES The views, opinions and/or findings contained in this report are those of the author(s) and should not be construed as an official Department of the Army position, policy or decision, unless so designated by other documentation.					
14. ABSTRACT Magnesium (Mg) is an attractive material for many lightweight applications because of its low density. Mg has a hexagonal close-packed (HCP) crystal structure with only 2 active slip systems available at room temperature for plastic deformation; therefore, it has poor room-temperature ductility and formability. As a result, Mg alloy components are manufactured via casting or elevated-temperature forming, processes that are time- and energy-consuming. Several approaches to improve the ductility of Mg alloys involve the use of rare-earth elements that are costly and may not be strategically available.					
15. SUBJECT TERMS magnesium alloys, room-temperature ductility, nano-sized precipitates					
16. SECURITY CLASSIFICATION OF:		17. LIMITATION OF ABSTRACT		15. NUMBER OF PAGES	19a. NAME OF RESPONSIBLE PERSON
a. REPORT UU	b. ABSTRACT UU	c. THIS PAGE UU	UU		Semyon Vaynman
				19b. TELEPHONE NUMBER 847-491-4475	

Report Title

Final Report: Research Area 11.1: HCP Mg Alloys Formable at Room Temperature

ABSTRACT

Magnesium (Mg) is an attractive material for many lightweight applications because of its low density. Mg has a hexagonal close-packed (HCP) crystal structure with only 2 active slip systems available at room temperature for plastic deformation; therefore, it has poor room-temperature ductility and formability. As a result, Mg alloy components are manufactured via casting or elevated-temperature forming, processes that are time- and energy-consuming. Several approaches to improve the ductility of Mg alloys involve the use of rare-earth elements that are costly and may not be strategically available.

It was demonstrated in this project that addition of lithium to Mg or formation of nano-sized precipitates improves the ductility of the alloys at room temperature: after specific heat-treatment, these Mg alloy plates did not form cracks when bent on themselves 180° around a mandrel at room temperature. The ductilization model for Mg alloys was developed. The improvement in ductility at room temperature is related to the interaction between solute atoms/clusters/nano-precipitates with screw dislocations that reduces the Peirls stress and activates additional slip systems for plastic deformation. This model could be applicable to other metals with limited number of slip systems for plastic deformation.

Enter List of papers submitted or published that acknowledge ARO support from the start of the project to the date of this printing. List the papers, including journal references, in the following categories:

(a) Papers published in peer-reviewed journals (N/A for none)

<u>Received</u>	<u>Paper</u>
-----------------	--------------

TOTAL:

Number of Papers published in peer-reviewed journals:

(b) Papers published in non-peer-reviewed journals (N/A for none)

<u>Received</u>	<u>Paper</u>
-----------------	--------------

TOTAL:

Number of Papers published in non peer-reviewed journals:

(c) Presentations

Number of Presentations: 0.00

Non Peer-Reviewed Conference Proceeding publications (other than abstracts):

Received Paper

TOTAL:

Number of Non Peer-Reviewed Conference Proceeding publications (other than abstracts):

Peer-Reviewed Conference Proceeding publications (other than abstracts):

Received Paper

TOTAL:

Number of Peer-Reviewed Conference Proceeding publications (other than abstracts):

(d) Manuscripts

Received Paper

TOTAL:

Number of Manuscripts:

Books

Received Book

TOTAL:

Received

Book Chapter

TOTAL:

Patents Submitted

Patents Awarded

Awards

Graduate Students

<u>NAME</u>	<u>PERCENT SUPPORTED</u>
FTE Equivalent:	
Total Number:	

Names of Post Doctorates

<u>NAME</u>	<u>PERCENT SUPPORTED</u>
FTE Equivalent:	
Total Number:	

Names of Faculty Supported

<u>NAME</u>	<u>PERCENT SUPPORTED</u>	National Academy Member
Semyon Vaynman	0.18	
Yip-Wah Chung	0.02	
Dieter Isheim	0.04	
FTE Equivalent:	0.24	
Total Number:	3	

Names of Under Graduate students supported

<u>NAME</u>	<u>PERCENT SUPPORTED</u>
FTE Equivalent:	
Total Number:	

Student Metrics

This section only applies to graduating undergraduates supported by this agreement in this reporting period

The number of undergraduates funded by this agreement who graduated during this period: 0.00

The number of undergraduates funded by this agreement who graduated during this period with a degree in science, mathematics, engineering, or technology fields:..... 0.00

The number of undergraduates funded by your agreement who graduated during this period and will continue to pursue a graduate or Ph.D. degree in science, mathematics, engineering, or technology fields:..... 0.00

Number of graduating undergraduates who achieved a 3.5 GPA to 4.0 (4.0 max scale):..... 0.00

Number of graduating undergraduates funded by a DoD funded Center of Excellence grant for Education, Research and Engineering:..... 0.00

The number of undergraduates funded by your agreement who graduated during this period and intend to work for the Department of Defense 0.00

The number of undergraduates funded by your agreement who graduated during this period and will receive scholarships or fellowships for further studies in science, mathematics, engineering or technology fields:..... 0.00

Names of Personnel receiving masters degrees

NAME
Total Number:

Names of personnel receiving PHDs

NAME
Total Number:

Names of other research staff

NAME PERCENT SUPPORTED
FTE Equivalent:
Total Number:

Sub Contractors (DD882)

Inventions (DD882)

Scientific Progress

Technology Transfer

Table of content

	Page
Background and objective	1
Summary of the most important results	2
<i>MgLi Alloys</i>	2
<i>MgCaZn Alloy</i>	5
Ductilization of Mg alloys (interaction of misfit centers with dislocations)	10

List of figures

		Page
Figure 1.	Increase in CRSS of basal $\langle a \rangle$ slip with increased Li concentration as a function of temperature	1
Figure 2.	Decrease in CRSS of pyramidal $\langle c+a \rangle$ slip with increased Li concentration as a function of temperature	2
Figure 3.	3-DAP image of Mg-11.4 at. % Li alloy. Lithium atoms are shown as black dots, and magnesium atoms are not shown for clarity	2
Figure 4.	Calculated polythermal section of Mg-Ca-Zn system at a constant Ca-content of 0.6 wt.% (0.37 at.%)	5
Figure 5.	Optical micrograph of Mg-Ca-Zn alloy in WQ condition	10
Figure 6.	Age-hardening of Mg-0.37at.% Ca-0.34 at.% Zn alloy after WQ from 470°C	
Figure 7.	Bent MgCaZn specimens: a – alloy homogenized at 470°C for 4 hrs and WQ; b - alloy homogenized at 470°C for 4 hrs, WQ and aged for 1 hr at 200°C	
Figure 8.	Tensile curve for MgCaZn alloy homogenized at 470°C for 4 hrs and WQ	
Figure 9.	SEM of the fractured in tensile test MgCaZn alloy homogenized at 470°C for 4 hrs and WQ	
Figure 10.	Figure 10. 3D APT of nano-sized Mg-Ca-Zn-rich precipitates in (a) an alloy that was homogenized at 470°C for 4 hrs and water quenched, and (b) in an alloy that was homogenized followed by aging for 1 hr at 200°C	
Figure 11.	Concentration profile of a nano-sized Mg-Ca-Zn precipitate in an alloy that was homogenized followed by aging for 1 hr at 200°C	
Figure 12.	3DAP maps of Mg, Ca, and Zn for Mg-0.3at.%Ca-0.3at.%Zn alloy aged for 60 ks at 200°C [33]	
Figure 13.	Flow stress at constant strain rate vs temperature	
Figure 14.	Double-kink mechanism for moving a screw dislocation with high Peierls stress from one energy valley to the next [23]. (a) Original position of screw dislocation parallel to a Peierls valley. (b) Screw position after a jog is thrown over a Peierls hill into a neighboring valley (formation of double kink). (c) After expansion under stress of	

	the double kink in (b)	
Figure 15.	J. Weertman's mechanism for the local reduction of Peierls stress caused by a nearby misfit center [24]. (a) Initial position. Formation of jogs (double kinks) at A and C (in the vicinity of misfit centers) requires less energy than at B, where no misfit centers are present. (b) After expansion of two double kinks formed at A and C	
Figure 16.	A screw dislocation segment pinned at both ends in the vicinity of a misfit center (distance Z_0 above)	
Figure 17.	Minimum energy configuration of a dislocation segment originally in screw orientation pinned by obstacles spaced $80b$ apart in the presence of a spherical misfit center located at $20b$ above the center of the dislocation segment (all units in Burgers vectors b). The input conditions are given in the text	
Figure 18.	Misfit centers strengthen the steel at elevated temperatures but reduce the flow stress at low temperatures, thereby lowering the DBTT	
Figure 19.	Twisting of $\langle c+a \rangle$ screw dislocation with increased lithium concentration	

Background and objective

Magnesium (Mg) is an attractive material for many lightweight military, automotive, aerospace, and consumer applications because of its low density of 1.74 gm/cm^3 vs 2.70 gm/cm^3 for aluminum [1-4]. However, since Mg has a hexagonal close-packed (HCP) crystal structure, it has two intrinsic problems in manufacturing and application. Firstly, the room-temperature ductility is poor [5]. According to the von Mises-Taylor criterion, five independent slip systems need to be activated for homogeneous plastic deformation in a polycrystalline material without crack or void formation. For Mg, the prevalent deformation mode at room temperature is slip on the basal plane along the two $\langle a \rangle$ directions, resulting in only two independent slip systems, so the von Mises-Taylor criterion is not satisfied. That is the primary reason for the poor room-temperature ductility and formability of HCP Mg alloys. Secondly, due to the dominance of basal slip at room-temperature, grains rotate during deformation, resulting in magnesium alloys with predominantly basal plane texture and hence strongly anisotropic mechanical properties, which are often undesirable. As a result, Mg alloy components are manufactured *via* casting or elevated-temperature forming to activate other slip systems. The disadvantage of these methods is slower processing and higher energy consumption, thus raising the manufacturing cost and limiting market penetration.

Several approaches have been taken to overcome the inherent ductility limitation of Mg. One is to introduce nanoparticles. For example, de Cicco and co-workers [6] found that ultrasonic dispersion of 15 wt.% SiC nanoparticles into Mg-4Zn increases the ductility from 5 to 10%. Electron microscopy studies indicated that nanoscale SiC particles suppress the formation of microscale Mg_7Zn_3 and Mg_2Zn_3 precipitates in favor of a nanoscale MgZn_2 phase. Such redistribution of intermetallic phases was cited as the source of ductility improvement. We speculate that nanoparticle-matrix interfaces may also generate localized strain fields that reduce the activation barrier for dislocation motion in these Mg alloys. Regardless, one must question if ultrasonic dispersion of nanoscale particles in molten metals is readily amenable to large-scale manufacturing.

Another approach is to introduce rare-earth or transition-metal alloying elements. As early as 1959, it was known that Mg becomes rollable at room-temperature when alloyed with rare-earth elements [7]. Shear bands at $30\text{-}35^\circ$ angle to the rolling direction were observed and were suggested to act as softening regions enabling improved formability. Recent investigations by Sandlobes *et al.* [8] showed that addition of 3 wt.% yttrium (Y) to Mg increases the room-temperature ductility from 4% to almost 25% with little loss of strength. Texture and electron microscopy analysis reveal that Mg-3 wt.%Y exhibits a high activity of twinning and pyramidal $c + a$ slip. Activation of pyramidal slip provides a sufficient number of slip systems to satisfy the von Mises-Taylor criterion. These additional deformation modes result in much improved ductility, less pronounced basal texture, and more uniform deformation, thus making the alloy more amenable to forming operations. Addition of Gd achieves similar levels of ductility [9,10]. The major disadvantage of this approach is cost and strategic availability of rare-earth elements.

In 2001, Kawamura *et al.* reported a magnesium alloy with a nominal composition of $\text{Mg}_{97}\text{Zn}_1\text{Y}_2$ that exhibited remarkably high tensile yield strength of 610 MPa at 16% elongation [11]. This strength is coupled with the appearance of novel ternary precipitates exhibiting order with long periods along the c-axis of the hexagonal close-packed (hcp) Mg matrix [12]. Referred to as long-period stacking ordered (LPSO) structures, these precipitates and their high strength have since been observed in a variety of ternary Mg systems [13–21]. However, LPSO systems

typically contain at least 1 at.% rare earth (RE) elements, making such alloys too expensive for high-volume industrial applications. In addition, most of these alloys were produced by rapid solidification and powder metallurgy. These manufacturing methods are not readily amenable to mass production of inexpensive and reliable Mg alloy components.

Another method to improve the room-temperature ductility is formation of very fine-grained alloy (2-4-micron grain size) by extrusion at elevated temperature (100-300°C) and addition of solid solution alloying elements [22]. The mechanism of ductility improvement is attributed by these authors to grain boundary compatibility stress that can operate in the entire grain volume to strongly promote the activation of basal and non-basal dislocation slips into the grain interiors.

The main objective of this exploratory project is to investigate the ductilization of Mg alloys by the formation of nano-sized precipitates or clusters and to develop a ductilization model with the ultimate goal to create new commercially useful Mg-based alloys with superior room-temperature ductility and formability that could be produced by conventional methods, and are formable at room temperature without the use of rare-earth elements.

The primary strategy of this work is based on the work of J. Weertman [23,24], who showed that the coherency strain at the precipitate (cluster)-matrix interface produces a torque on nearby screw dislocations, thereby improving ductility through locally reducing the Peierls stress, resulting in increased dislocation mobility and hence more available slip systems. We demonstrated the occurrence of this phenomenon by significantly enhancing the low-temperature fracture properties of steels by the formation of nanometer-sized precipitates (clusters) in the steel matrix [25]. We are extending this concept to the design of Mg alloys. Two alloys were studied in this exploratory project: Mg-Li and Mg-Ca-Zn.

Summary of the most important results

MgLi Alloys

Improvement of mechanical properties and room-temperature ductility of magnesium alloy with an addition of lithium is well known[26-30]. To understand the reason why it happens, a study of tensile properties of Mg-Li single crystals with Li from 1.5 to 15 at. % were performed at Northwestern University [31]. These single crystals were produced by the Bridgman technique and then cut into tensile specimens in the specific crystallographic direction using back reflection Laue method.

Tensile tests demonstrated that the addition of lithium to magnesium alloys increased the critical resolved shear stress (CRSS) in the basal plane but softened the alloy with respect to glide in prismatic and pyramidal planes. For example, the addition of 6.0 at. %-Li at 300°K increased the CRSS for basal slip by a factor of five (Figure 1). This behavior was corroborated by Han *et al.* who used density functional theory to calculate generalized stacking fault energies in the basal plane [32]. In the pyramidal plane, for example, the addition of 7.5 at. %-Li at 300°K decreased the CRSS by a factor of two (Figure 2). Therefore, addition of Li to Mg results in alloy strengthening and in the same time increased ductility by activating pyramidal slip.

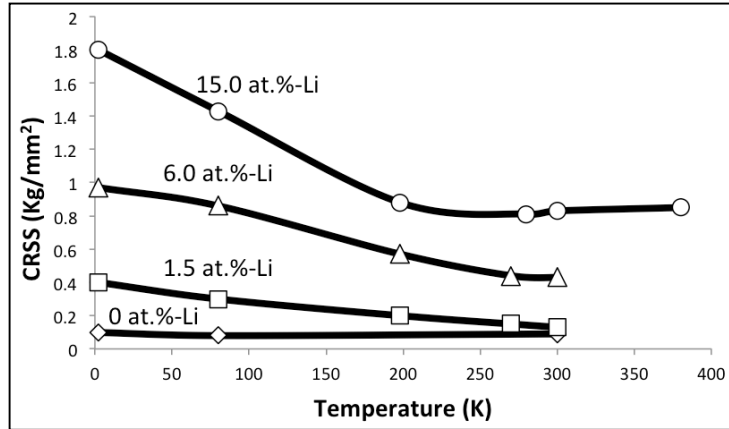


Figure 1. Increase in CRSS of basal $\langle a \rangle$ slip with increased Li concentration as a function of temperature

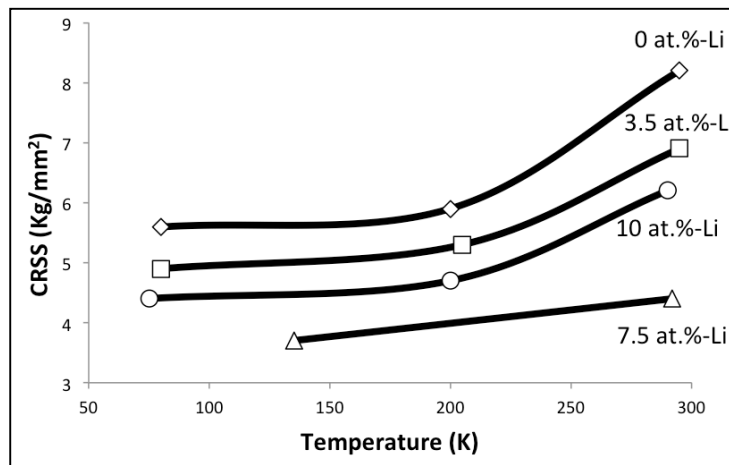


Figure 2. Decrease in CRSS of pyramidal $\langle c+a \rangle$ slip with increased Li concentration as a function of temperature

We used 3D Atom Probe Tomography to analyze Mg-Li single crystal alloys of varying compositions from 1.4 to 11.4 at. % Li. Figure 3 is a 3-D reconstruction of a Mg-11.4 at. % Li alloy sample, with only the lithium atoms shown for clarity. From visual inspection, lithium appears to be evenly dispersed throughout the sample. All other Mg-Li samples exhibited lithium distributions qualitatively similar to the one shown in Figure 3.

Detailed pair correlation distribution analysis of the above 3DAP data was performed, showing that lithium solute atoms are nearly randomly distributed. This suggests that the solid-solution hardening and softening in different crystallographic planes is a local effect stemming from distortions induced by single or small clusters of lithium atoms in the HCP magnesium crystal structure. Basal plane hardening can be attributed to normal solid solution hardening, while solid solution softening in the pyramidal plane can be attributed to lithium dislocation motion as proposed by Weertman [23,24] and described below.

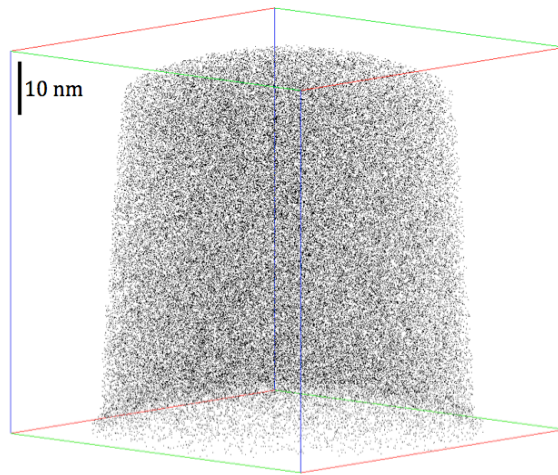


Figure 3. 3-DAP image of Mg-11.4 at. % Li alloy. Lithium atoms are shown as black dots, and magnesium atoms are not shown for clarity

MgCaZn Alloy

We previously discovered that under-aged Mg-0.37 at. % Ca-0.34 at. % Zn alloy is very ductile. This section describes the mechanical and microstructural properties of this alloy.

Thermodynamic modeling of Mg-Ca-Zn performed at Northwestern University indicates binary and ternary intermetallic precipitates can be formed by solution treatment of alloy above 470°C followed by water quenching and aging, as shown in the polythermal section of the phase diagram at a constant Ca content of 0.6 wt.% (0.37 at.%) in Figure 4.

The alloy was melted in an inert atmosphere and then cast into 100-mm wide, 12-mm thick, 150-mm high mold by Sophisticated Alloys, Inc. The cast was cut into slices, homogenized in an argon atmosphere for 4 hrs at 470°C and then water-quenched (WQ). The microstructure of the alloy in as-WQ condition is shown in Figure 5. The alloy is coarse-grained.

The alloy was aged at 150, 180 and 200°C in air. It is obvious that this alloy age-hardens significantly (Figure 6). The micro-hardness increased from about 55 Vickers to approximately 75 Vickers at the peak hardness, indicating formation of precipitates (clusters).

To quickly determine if alloy is ductile or brittle after different heat-treatments, approximately 1 mm-thick slices were cut from the alloy blocks and hand-bent around a rod (5 mm diameter). Some specimens broke in a brittle manner, while others were quite ductile, bending without crack formation. Optical and scanning electron microscopy of fracture surfaces clearly indicated grain boundary oxidation in the brittle specimens. Oxidation of the original alloy ingot is clearly a problem. The material was reordered, but the new ingot had the same oxidation problem. The project was continued with the received material.

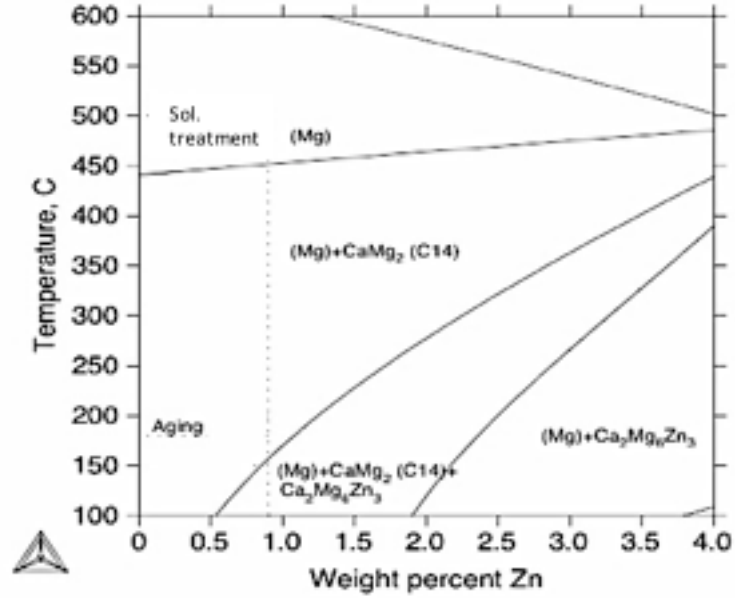


Figure 4. Calculated polythermal section of Mg-Ca-Zn system at a constant Ca-content of 0.6 wt.% (0.37 at.%)

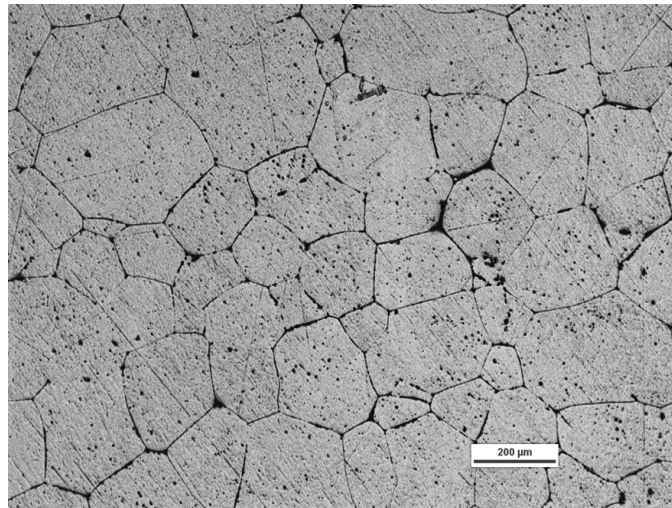


Figure 5. Optical micrograph of Mg-Ca-Zn alloy in WQ condition

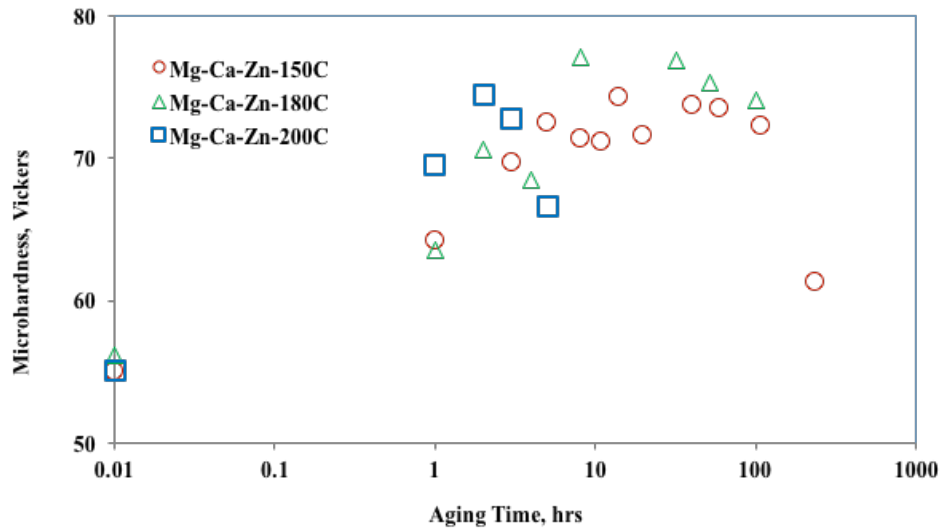


Figure 6. Age-hardening of Mg-0.37at.% Ca-0.34 at.% Zn alloy after WQ from 470°C

We found that the alloy is very ductile after WQ (Figure 7a). When the alloy was aged at 200°C for more than 10 minutes, it became brittle. Figure 7b shows the fractured specimen aged at 200°C for 1 hr.

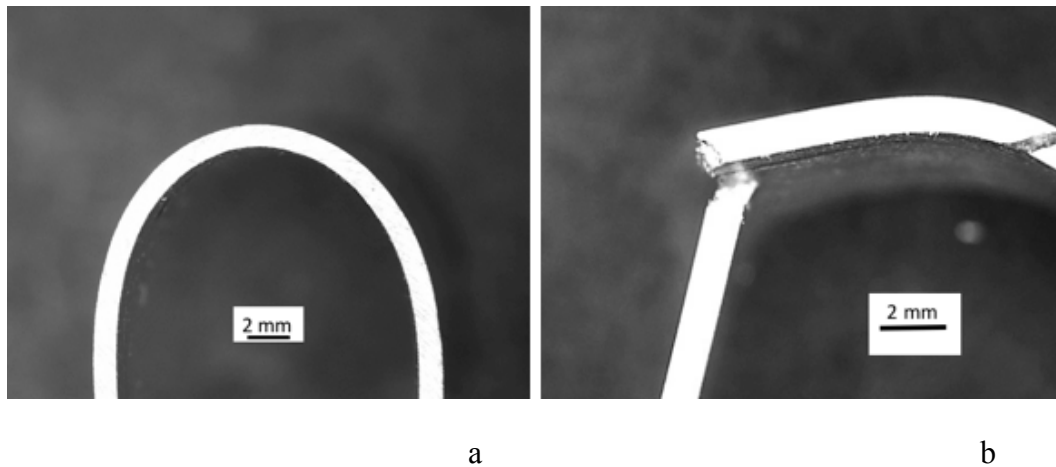


Figure 7. Bent MgCaZn specimens: a – alloy homogenized at 470°C for 4 hrs and WQ; b - alloy homogenized at 470°C for 4 hrs, WQ and aged for 1 hr at 200°C

Tensile testing was performed on alloy homogenized at 470°C for 4 hrs and WQ. Due to the inhomogeneity of the alloy, we could not tell in advance if specimens will be machined from “good” (less oxidized) or “bad” (oxidized) sections of the material. When tested, oxidized samples fractured during the elastic deformation, while less oxidized samples exhibited plastic deformation and failed at around 4%, well below expected values. The tensile curve for the second specimen is shown in Figure 8.

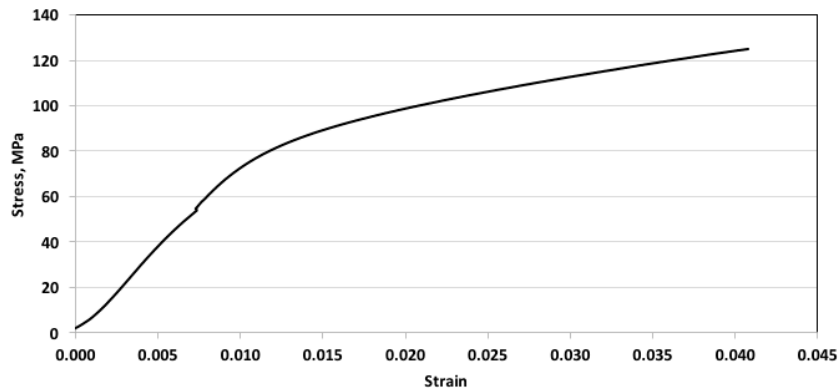


Figure 8. Tensile curve for MgCaZn alloy homogenized at 470°C for 4 hrs and WQ

Figure 9 shows an SEM image of the fractured surface of the second tensile specimen. It is obvious that the failure is mixed; while there is some cleavage and ductile fracture, the specimen failed mostly due to intergranular fracture. It appears that weak grain boundary cohesion resulted from poor alloy production, due most likely to grain boundary oxidation.

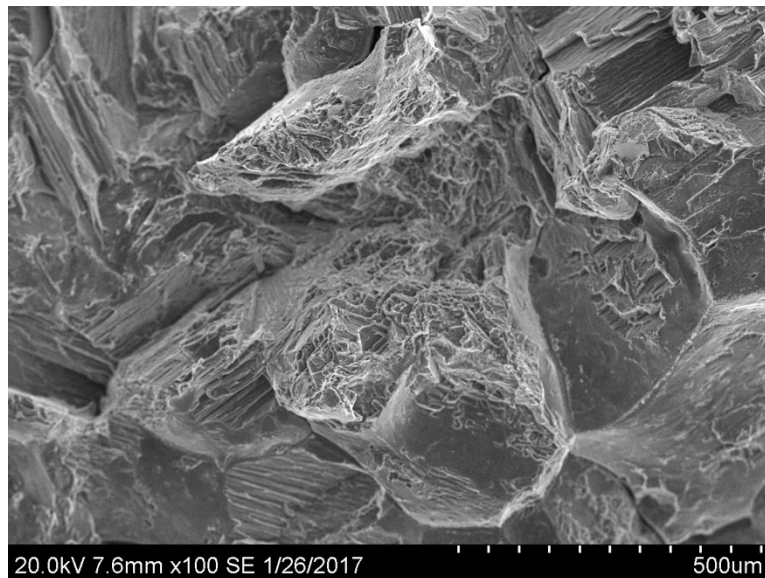


Figure 9. SEM of the fractured in tensile test MgCaZn alloy homogenized at 470°C for 4 hrs and WQ

3D Atom Probe Tomography (APT) of MgCaZn alloy was performed to follow precipitation processes that can significantly affect the mechanical properties. One sample was homogenized at 470°C for 4 hrs and water quenched (ductile) and the second sample was heat-treated as first and then aged for 1 hr at 200°C (brittle). It is obvious that nano-sized precipitates or GP zones enriched in Zn and Ca have formed on water quenching (Figure 10a) with a very high number density. When alloy is aged (Figure 10b), precipitates coarsen. It seems that precipitates with aging time have a tendency to elongate and align with specific crystallographic orientations of the matrix.

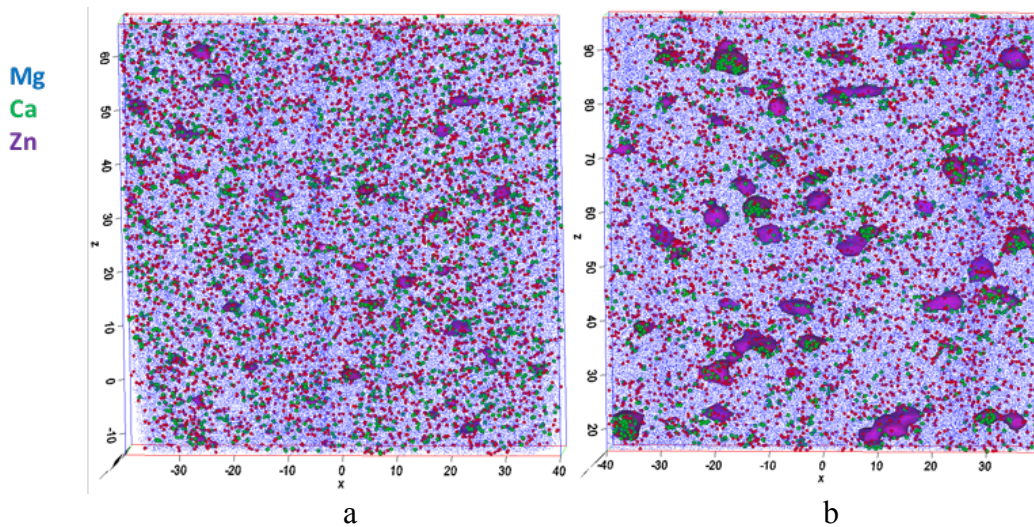


Figure 10. 3D APT of nano-sized Mg-Ca-Zn-rich precipitates in (a) an alloy that was homogenized at 470°C for 4 hrs and water quenched, and (b) in an alloy that was homogenized followed by aging for 1 hr at 200°C

A concentration profile across a precipitate in the alloy aged for 1 hr at 200°C is shown in Figure 11. The maximum elemental concentrations observed in this profile are 9.4 at.% Ca and 7.2 at.% Zn.

In the past some 3D APT of similar MgCaZn alloys was performed, but no formation of the rounded nano-sized precipitates was reported [33]. The MgCaZn GP zones (plates) were formed as seen in Figure 12 for this alloy aged at 200°C for very long time, 60,000 sec (16.7 hrs).

It seems that the transition from ductile to brittle failure in MgCaZn alloy occurs due to the coarsening of the nano-sized precipitates and alignment of larger precipitates along specific crystallographic planes. More detailed 3D APT and TEM studies are needed

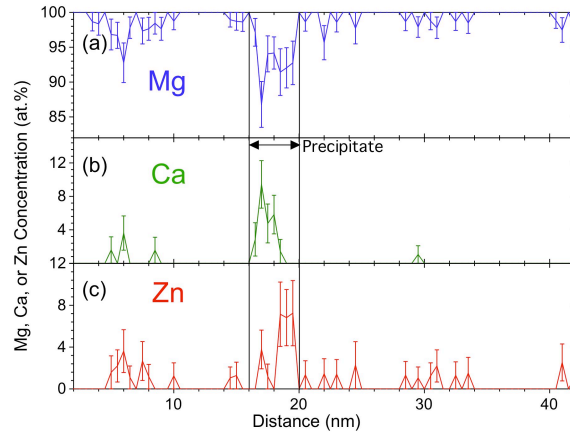


Figure 11. Concentration profile of a nano-sized Mg-Ca-Zn precipitate in an alloy that was homogenized followed by aging for 1 hr at 200°C

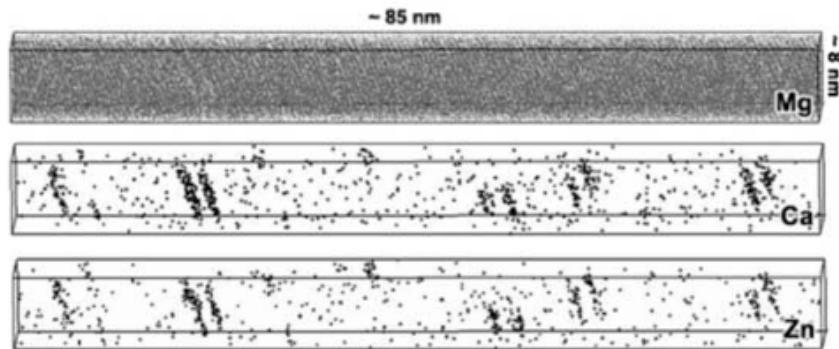


Figure 12. 3DAP maps of Mg, Ca, and Zn for Mg-0.3at.%Ca-0.3at.%Zn alloy aged for 60 ks at 200°C [33]

Ductilization of Mg alloys (interaction of misfit centers with dislocations)

In general, the ductile-to-brittle transition in metals depends on the interplay between flow stress and fracture stress (Figure 13). In steels and many alloys, the mobility of screw dislocations and consequently the flow stress depend strongly on temperature and strain rate; flow stress increases as temperature is decreased. In contrast, the fracture stress is almost independent of temperature and strain rate (except for some minor temperature dependence of modulus [34] and its possible effect on fracture stress). At high temperatures (usually above room temperature) and low strain rates, thermal energy is sufficient to activate the motion of screw dislocations, resulting in plastic flow at stresses below the fracture stress. However, as one lowers the temperature, less thermal energy is available, and higher stress is required to activate the motion of screw dislocations. Therefore, the flow stress increases with decreasing temperature. Eventually, the flow stress curve intersects the fracture stress at a critical temperature, below which the metal suffers brittle fracture before yielding. This is the ductile-to-brittle transition temperature (DBTT) as shown in Figure 13. For Mg and its alloys DBTT is

significantly above room temperature because there is only two independent slip system for Mg and its alloys at room temperature. At elevated temperatures, more slip systems are activated, thus Mg and alloys become ductile.

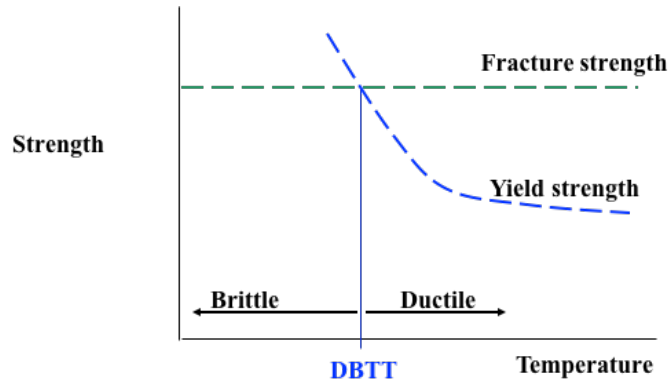


Figure 13. Flow stress at constant strain rate vs temperature

The stress (Peierls stress) to move a long dislocation segment from a crystallographic energy valley in BCC (ferritic steels) and HCP (Mg and alloys) metals is large. J. Weertman proposed many years ago that a high Peierls energy dislocation likely would move by first forming a double kink [23] (Figure 14). Subsequently, J. Weertman suggested that a solute atom or a cluster of solute atoms may act as a misfit center that interacts with a dislocation to help pull it from its Peierls energy valley [24] (Figure 15) by lowering Peierls stress.

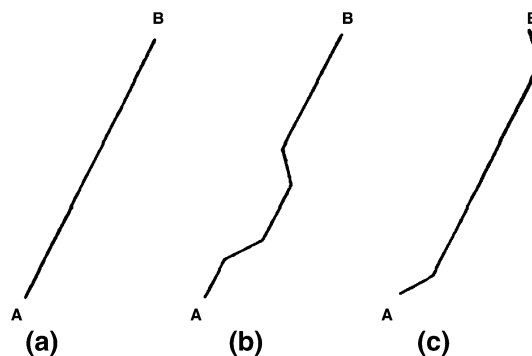


Figure 14. Double-kink mechanism for moving a screw dislocation with high Peierls stress from one energy valley to the next [23]. (a) Original position of screw dislocation parallel to a Peierls valley. (b) Screw position after a jog is thrown over a Peierls hill into a neighboring valley (formation of double kink). (c) After expansion under stress of the double kink in (b).

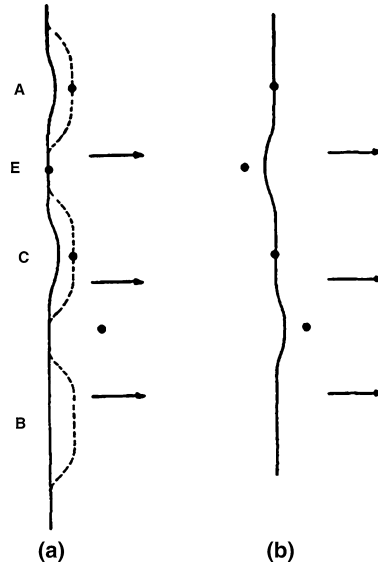


Figure 15. J. Weertman's mechanism for the local reduction of Peierls stress caused by a nearby misfit center [24]. (a) Initial position. Formation of jogs (double kinks) at A and C (in the vicinity of misfit centers) requires less energy than at B, where no misfit centers are present. (b) After expansion of two double kinks formed at A and C

Urakami and Fine [35] developed a mathematical treatment of the effect of a solute atom or solute cluster misfit center on a nearby dislocation segment pinned at both ends in the spirit of Weertman's idea. Their treatment is presented here in detail, using the geometry shown in Figure 16.

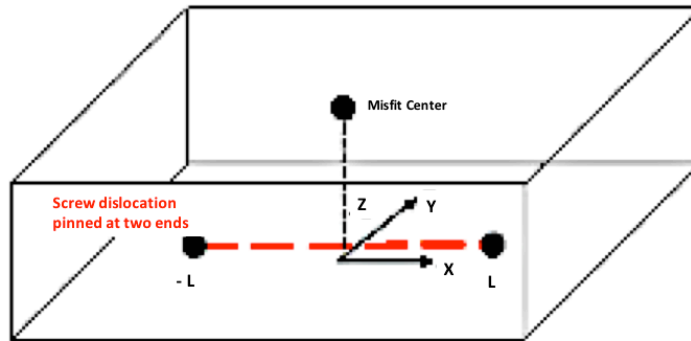


Figure 16. A screw dislocation segment pinned at both ends in the vicinity of a misfit center (distance Z_0 above)

The energy I of the screw dislocation in the presence of a misfit center is expressed as follows:

$$I = \int \left[E(y) \sqrt{1 + \left(\frac{dy}{dx} \right)^2} - \int_0^y F(x, s) ds \right] dx \quad [1]$$

where $E(y)$ is the periodic Peierls potential energy per unit length of the screw dislocation, and F is the force of the misfit center acting on unit length of the screw dislocation. This integral is minimized when the integrand L (expression inside the square bracket) satisfies the following Euler–Lagrange equation:

$$\frac{\partial}{\partial x} \left(\frac{\partial L}{\partial p} \right) - \frac{\partial L}{\partial y} = 0 \quad [2]$$

where $p = \frac{dy}{dx}$

L is a function of x , $y(x)$, and dy/dx . Direct computation reduces the Euler–Lagrange equation to the following:

$$E(y) \frac{dp}{dx} \frac{1}{(1+p^2)^{3/2}} - \frac{\partial E}{\partial y} \frac{1}{(1+p^2)^{1/2}} + F(x, y) = 0 \quad [3]$$

For simplicity, we will assume that the Peierls valleys vary with a period equal to the Burgers vector b as follows:

$$E(y) = E_0 - A \cos\left(\frac{2\pi y}{b}\right) \quad [4]$$

The term $F(x, y)$, the force acting on a unit length of the dislocation resulting from the misfit center, is expressed as follows:

$$F(x, y) = \frac{6\mu b \varepsilon V z_0 x}{(x^2 + y^2 + z^2)^{5/2}} \quad [5]$$

where μ is the shear modulus, b is the Burgers vector, ε is the misfit strain, V is the volume of the misfit center, and z_0 is the position of the misfit center above the glide plane. To simplify, we will express everything in dimensionless quantities as follows:

$$E_R = \frac{E_0}{\mu b^2} \quad A_R = \frac{A}{\mu b^2} \quad S = \frac{V}{b^3}$$

In addition, we will normalize lengths by the following Burgers vector:

$$L_R = \frac{L}{b} \quad x_R = \frac{x}{b} \quad y_R = \frac{y}{b} \quad z_R = \frac{z_0}{b}$$

Equation [3] becomes the following:

$$[E_R - A_R \cos(2\pi y_R)] \frac{1}{(1+p^2)^{3/2}} \frac{dp}{dx_R} + \frac{1}{(1+p^2)^{1/2}} 2\pi A_R \sin(2\pi y_R) + \frac{6S z_R x_R}{(x_R^2 + y_R^2 + z_R^2)^{5/2}} = 0 \quad [6]$$

Typically, $0.2 < E_R < 1.0$ and $10^6 < A_R < 10^3$. The Peierls stress is $2\pi\mu A_R$

Equation [6] can be solved numerically for given input values of L_R , E_R , A_R , z_R , and S . To illustrate, we will assume that the dislocation segment is pinned by obstacles spaced $80b$ apart. The misfit center is located at $20b$ above the middle of the dislocation segment. As a reference, $S = 1.0$ corresponds approximately to a spherical precipitate with a radius equal to $5b$ and a misfit strain of 0.2 pct. E_R and A_R are set to 0.5 and 5×10^{-5} , respectively. The result is shown in Figure 16 for $S = 0.5, 1.0,$ and 2.0 . In the absence of thermal energy and with a given sinusoidal Peierls potential, the stress to move the dislocation is a maximum at $b/4$ from the Peierls valley. Therefore, if the effect of the misfit center is large enough to twist the dislocation locally by $b/4$, then the dislocation will move spontaneously to the next valley, forming a kink (Figure 17). For the previous input conditions, the maximum twisting of the screw dislocation is between $0.07b$ and $0.22b$ as S varies from 0.5 to 2.0. This is a significant fraction of $b/4$. Thus, the Peierls stress needed for the screw segment to jump spontaneously into the next Peierls valley has been reduced.

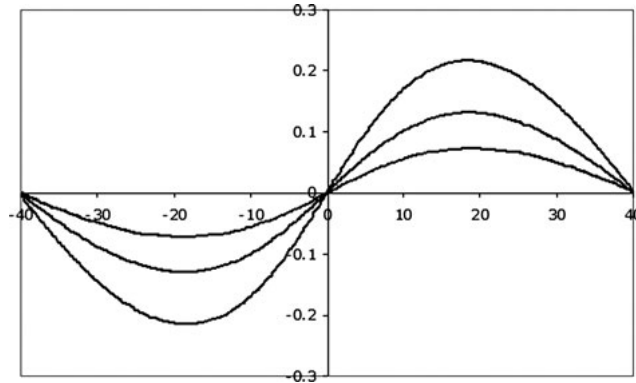


Figure 17. Minimum energy configuration of a dislocation segment originally in screw orientation pinned by obstacles spaced $80b$ apart in the presence of a spherical misfit center located at $20b$ above the center of the dislocation segment (all units in Burgers vectors b). The input conditions are given in the text.

The previous calculations demonstrate that a nearby misfit center indeed may provide sufficient twisting of a screw dislocation to reduce the activation energy for plastic flow. In the MgCaZn alloy studied in this project, the nanoscale precipitates are misfit centers. These nanoscale precipitates seem to have dual roles; they increase the flow stress at higher temperature because of precipitation strengthening, but they decrease the flow stress at lower temperatures because of the interaction between stress fields of these misfit centers with nearby screw dislocations. As depicted in Figure 18, this interaction leads to a flatter temperature dependence of flow stress and consequently to a lower DBTT.

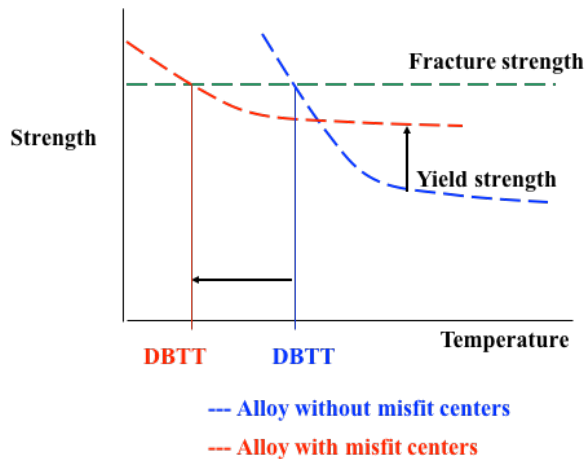


Figure 18. Misfit centers strengthen the steel at elevated temperatures but reduce the flow stress at low temperatures, thereby lowering the DBTT

In the case of MgLi alloys, Li solute atoms were assumed to be misfit centers. Higher lithium content implies smaller average distance between misfit centers and dislocations. Figure 19 shows that higher lithium concentration results in stronger twisting of a nearby dislocation and hence better ductility, as observed experimentally.

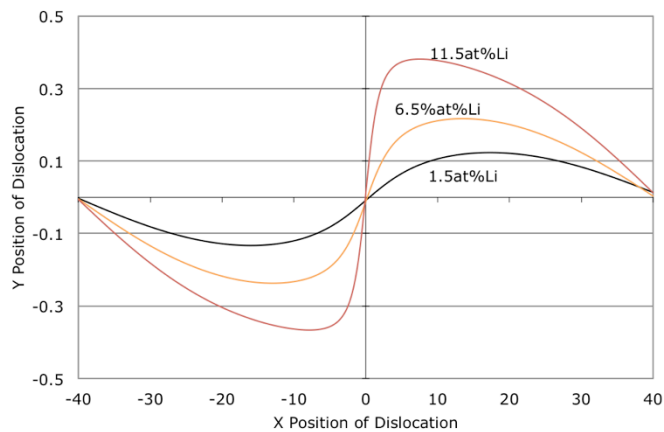


Figure 19. Twisting of $\langle c+a \rangle$ screw dislocation with increased lithium concentration

It appears that for MgLi alloys, reduction of CRSS in $\langle c+a \rangle$ pyramidal slip is a consequence of reduced distance between misfit center and dislocation line, not an increase of misfit radius (solute clustering). The Weertman model assumes a spherical strain field due to the misfit center. This may not be strictly correct for the Mg-Li system. It is known experimentally that addition of lithium to Mg decreases the c/a ratio from 1.623 to 1.610, suggesting an anisotropic distortion. This non-uniform contraction of the c and a axis also suggests increased atomic density in the prismatic plane that could allow for easier dislocation movement in non-basal planes.

Therefore, the increased ductility in MgLi systems can be attributed to the activation of pyramidal $\langle c+a \rangle$ slip systems by lithium solute atoms, providing enough slip systems for ductile deformation. In addition, lithium solutes reduce the disparity in CRSS between basal and non-basal slip systems, promoting isotropy and uniform elongation.

We demonstrate theoretically that coherent and coplanar misfit centers such as nanoscale precipitates in MgCaZn alloy and single Li atoms in MgLi can provide sufficient twisting of nearby screw dislocations to enhance their mobility in the absence of insufficient thermal activation. This mechanism activates additional slip systems leading to significant improvement of ductility in Mg alloys at room temperature. The aging of the MgCaZn alloy resulting in lower ductility is likely due to precipitate coarsening and hence loss of coherency. This should be studied in detail.

The presented ductility improvement model opens a new paradigm for the design of more ductile Mg alloys by formation of misfit centers (solute atoms/clusters/nano precipitates), as well as a way to decrease the DBTTs in other bcc and hcp metals, and related intermetallics.

Bibliography

1. M. Gupta and N.M.L. Sharon, *Magnesium, Magnesium Alloys, and Magnesium Composites*, John Wiley & Sons, Hoboken, NJ (2011).
2. H.E. Friedrich and B.L. Mordike (eds.), *Magnesium Technology - Metallurgy, Design Data, Applications*, Springer-Verlag, Berlin, Germany (2006).
3. K.U. Kainer (ed.) *Magnesium – Alloys and Technologies*, Wiley-VCH Verlag GmbH, Heidelberg, Germany (2003).
4. P. D. Frost, *Technical and Economic Status of Magnesium-Lithium Alloys*, NASA SP-5028 (1965).
5. S. R. Agnew, M. H. Yoo, and C. N. Tome, *Acta Mater.* 49, 4277 (2001).
6. M. de Cicco, H. Konishi, H. Konishi, G. Cao, H. S. Choi, L-S. Turng, J. H. Perepezko, S. Kou, R. Lakes, and X. Li, *Metall. Mat. Trans.* 40A, 3038 (2009).
7. S. L. Couling, J. F. Pashak, and L. Sturkey, *Trans ASM* 51, 94 (1959).
8. S. Sandlobes, S. Zaefferer, I. Schestakow, S. Yi, and R. Gonzalez-Martinez, *Acta Mater.* 59, 429 (2011).
9. S. M. He, X. Q. Zeng, L. M. Peng, X. Gao, J. F. Nie, and W. J. Ding, *J. Alloys & Compounds* 427, 316 (2007).
10. N. Stanford, I. Sabirov, G. Sha, A. La Fontaine, S. P. Ringer, and M. R. Barnett, *Met. Mater Trans* 41A, 734 (2010).
11. Y. Kawamura, K. Hayashi, A. Inoue, T. Masumoto, *Mater Trans* 42, 1172, (2001).
12. A. Inoue, Y. Kawamura, M. Matsushita, K. Hayashi, J. Koike, *J Mater Res* 16, 189 (2001).
13. K. Amiya, T. Ohsuna, A. Inoue, *Mater Trans* 44, 2151 (2003).
14. M. Yamasaki, T. Anan, S. Yoshimoto, Y. Kawamura, *Scripta Mater*, 53, 799(2005).
15. Kawamura Y, Kasahara T, Izumi S, Yamasaki M. *Scripta Mater*, 55, 453 (2006).
16. K. Yamada, Y. Okubo, M. Shiono, H. Watanabe, *Mater Trans*, 47, 1066 (2006).
17. Kawamura Y, Yamasaki M. *Mater Trans*, 48, 2986, (2007).
18. T. Itoi, K. Takahashi, H. Moriyama, M. Hirohashi, *Scripta Mater*, 59, 1155 (2008).
19. J. Nie, K. Ohishi, X. Gao, K. Hono, *Acta Mater*, 56, 6061 (2008).

20. H. Yokobayashi, K. Kishida, H. Inui, M. Yamasaki, Y. Kawamura, *Acta Mater*, 59, 7287 (2011).
21. S-B. Mi, Q-Q Jin, *Scripta Mater* 68, 635 (2013).
22. H. Somekawa, A. Singh, T. Mukai, T. Inoue, *Phil. Mag.*, 96, 2671 (2016).
23. J. Weertman, *Phys. Rev*, 101, 1429 (1956).
24. J. Weertman, *J. Appl. Phys*, 29, 1685 (1958).
25. M. E. Fine, S. Vaynman, D. Isheim, Y. W. Chung, S. P. Bhat, and C. H. Hahin, *Metall. Mat. Trans.* 41A, 3318 (2010).
26. F.E. Hauser, P.R. Landon, J.E. Dorn, *Trans. ASM*, 48, 986 (1956).
27. G.V. Raynor, *The Physical Metallurgy of Magnesium and its Alloys*, Pergamon, New York (1959).
28. C.S. Roberts, *Magnesium and Its Alloys*, John Wiley, New York (1960).
29. E.F. Emley, *Principles of Magnesium Metallurgy*, Pergamon, New York (1966).
30. P. Metenier, G. Gonzales-Dongel, O.A. Ruano, J. Wolfenstine, O.D. Sherby, *Mat. Sci. & Eng*, A125, 195 (1989).
31. A. Urakami, M. Meshii, M.E. Fine, in: *Second International Conference On The Strength of Metals and Alloys*, American Society For Metals, Asilomar Conference Grounds (1970).
32. Han, X.M. Su, Z.H. Jin, Y.T. Zhu, *Scripta Mat.*, 64, 693 (2010).
33. J.C. Oh, T. Ohkubo, T. Mukai, K. Hono, *Scripta Mat.*, 53, 675 (2005).
34. G.R. Speich, A.J. Schwoeble, and W.C. Leslie: *Metall. Trans.*, 22, 2031 (1972).
35. A. Urakami and M.E. Fine: *Scripta Metall.*, 4, 667 (1970).